ORIGINAL ARTICLE

Expression of α-Defensins, CD20+ B-lymphocytes, and Intraepithelial CD3+ T-lymphocytes in the Intestinal Mucosa of Patients with Liver Cirrhosis: Emerging Mediators of Intestinal Barrier Function

Georgios I. Tsiaoussis[1] · Eleni C. Papaioannou[2] · Eleni P. Kourea[2] · Stelios F. Assimakopoulos[3] ·
Georgios I. Theocharis[1] · Michalis Petropoulos[5] · Vasileios I. Theopistos[1] · Georgia G. Diamantopoulou[1] ·
Zoi Lygerou[5] · Iris Spiliopoulou[4] · Konstantinos C. Thomopoulos[1]

Abstract

Aim The present study investigates the role of innate and adaptive immune system of intestinal mucosal barrier function in cirrhosis.

Methods Forty patients with decompensated ($n = 40$, group A), 27 with compensated cirrhosis ($n = 27$, group B), and 27 controls ($n = 27$, group C) were subjected to duodenal biopsy. Expression of α-defensins 5 and 6 at the intestinal crypts was evaluated by immunohistochemistry and immunofluorescence. Serum endotoxin, intestinal T-intraepithelial, and lamina propria B-lymphocytes were quantified.

Results Cirrhotic patients presented higher endotoxin concentrations ($p < 0.0001$) and diminished HD5 and HD6 expression compared to healthy controls ($p = 0.000287$, $p = 0.000314$, respectively). The diminished HD5 and HD6 expressions were also apparent among the decompensated patients compared to compensated group ($p = 0.025$, $p = 0.041$, respectively). HD5 and HD6 expressions were correlated with endotoxin levels (r = -0.790, $p < 0.0001$, r = −0.777, $p < 0.0001$, respectively). Although intraepithelial T-lymphocytes were decreased in group A compared to group C ($p = 0.002$), no notable alterations between groups B and C were observed. The B-lymphocytic infiltrate did not differ among the investigated groups.

Conclusions These data demonstrate that decreased expression of antimicrobial peptides may be considered as a potential pathophysiological mechanism of intestinal barrier dysfunction in liver cirrhosis, while remodeling of gut-associated lymphoid tissue as an acquired immune response to bio-pathogens remains an open field to illuminate.

Keywords Bacterial translocation · Mucosal defense · Antimicrobial peptides · Gut-associated lymphoid tissue · Endotoxin · Paneth cells

Introduction

The gastrointestinal tract beyond the primary function of digestion and nutrient absorption operates as a barrier to impede the penetration of harmful agents, including intraluminal bacteria and endotoxin and dissemination to distant organs and tissues [1]. The monolayer of intestinal epithelium plays a pivotal role as the first component of the gut mucosal barrier and normally limits microbial invasion. It consists of four distinct cell types: the columnar enterocytes that regulate the paracellular route by tight junctions [2], the mucin-secreting goblet cells [3], the hormone-secreting enteroendocrine cells, and the antimicrobial agent-secreting Paneth cells (PCs) [4].

✉ Georgios I. Tsiaoussis
tsiaoussisgeorgios@yahoo.com

1 Department of Gastroenterology, University Hospital of Patras, CP 26504 Patras, Greece

2 Department of Pathology, School of Medicine, University of Patras, CP 26504 Patras, Greece

3 Department of Internal Medicine, University Hospital of Patras, CP 26504 Patras, Greece

4 Department of Microbiology, School of Medicine, University of Patras, CP 26504 Patras, Greece

5 Department of General Biology, School of Medicine, University of Patras, CP 26504 Patras, Greece

Paneth cells are specialized zinc-containing epithelial cells and reside at the base of Lieberkühn's intestinal crypts [5, 6]. They produce, store in cytoplasmic granules, and secrete a broad spectrum of antimicrobial peptides (AMPs) most abundantly the human α-defensins 5, 6 (HD5, HD6), lysozyme, lectins, and phospholipase A2, contributing to gut barrier function [7–11].

Antimicrobial peptides constitute an integral component of the host innate immune system and are considered as broad-spectrum "natural antibiotics." They directly neutralize invading microorganisms, constituting the immunological barrier that protects a host from penetrating harmful bacteria [12, 13].

Defensins are cationic peptides containing three intramolecular disulfide bonds with a broad spectrum of antimicrobial activity against Gram-negative and Gram-positive bacteria, fungi, viruses, and protozoa [14–17]. They can form pores in the microbial membranes, leading to disruption of the membrane integrity of target microbes [18]. Intestinal HD5 provides broad-spectrum microbicidal activity, and HD6 blocks the attachment of potentially pathogenic luminal organisms to the epithelial cell monolayer, to successfully prevent enteric infection, thus contributing to the enteric innate mucosal immunity [19, 20].

Cirrhosis-associated immune dysfunction syndrome (CAIDS) is multifactorial, resulting in loss of the immunosurveillance ability and intestinal barrier dysfunction with detrimental effects in clearing bacteria and endotoxins [21].

Generally, it is considered that intestinal intraepithelial lymphocytes (IELs) play a crucial role in the gut mucosal immune system and exert an immune protective effect against microbial infection by a variety of immunoregulatory functions, including cytokine production and cytotoxic activity [22–25]. However, data on the gut-associated lymphoid tissue (GALT) in cirrhosis are sparse, especially at the tissue level.

This study focuses on the role of Paneth cell α-defensins in innate mucosal immunity of the small intestine as well as the specific GALT changes, concerning the intestinal CD3+ IELs and CD20+ B-lymphocytes within lamina propria, as an adaptive immune mechanism of mucosal barrier function in cirrhosis.

Patients and Methods

Patients' Characteristics

Stable adult patients with decompensated (n = 40, median age 59.5 years) and compensated (n = 27, median age 61 years) cirrhosis and healthy subjects (n = 27, median age 58 years) were enrolled in the study. The etiology of cirrhosis was alcoholic liver disease in 32 patients, viral hepatitis

in 29 patients, and other causes in 6 patients. Baseline characteristics of the enrolled population are summarized in Table 1. The diagnosis of liver cirrhosis was established by means of histology and/or by its clinical, laboratory, endoscopic, or imaging manifestations. Cirrhosis severity was assessed according to the Child–Pugh and MELD-sodium score.

Eligibility criteria were as follows: patients of either sex over 18 years old with a definite diagnosis of liver cirrhosis. Exclusion criteria included malignancy, extrahepatic biliary obstruction, uncontrolled diabetes mellitus, renal failure, gastrointestinal diseases (celiac disease, pancreatitis, inflammatory bowel disease, gastrointestinal bleeding in the last 4 weeks), intestinal surgery, current infections, including spontaneous bacterial peritonitis, alcohol abuse in the last

Table 1 Descriptive and clinical characteristics of cirrhotic patients

	Compensated (n = 27)	Decompensated (n = 40)	Overall cirrhotic patients (n = 67)
Gender			
Male	17	30	47
Female	10	10	20
CP score			
A	27	–	27
B	–	21	21
C	–	19	19
MELD-Na score			
≥ 20	–	16	16
< 20	–	24	24
Ascites			
Yes	–	40	40
No	27	–	27
Ascites grade			
G1	–	13	13
G2	–	20	20
G3	–	7	7
EV			
Yes	12	36	48
No	15	4	19
EV size			
F1	4	12	16
F2	6	9	15
F3	2	15	17
PHG			
Yes	9	30	39
No	18	10	28
Gastric varices			
Yes	1	6	7
No	26	34	60

CP score Child–Pugh score, *MELD* Model for End-Stage Liver Disease, *EV* esophageal varices, *PHG* portal hypertensive gastropathy

4 weeks, and treatment during the last month with medications that might affect endotoxin measurements. The control group (group C) comprised of healthy individuals, without any of the above-stated exclusion criteria, who underwent an upper gastrointestinal tract endoscopy without pathologic findings. Cirrhotic patients were subsequently divided into two groups: Child–Pugh A was classified as compensated cirrhosis (group B), whereas Child–Pugh B or C as decompensated cirrhosis (group A). All subjects enrolled in the study underwent an upper gastrointestinal tract endoscopy, during which biopsies from the second portion of the duodenum were obtained.

This prospective study was approved by the Ethics Research Committee of Patras University Hospital, Patras, Greece, and informed consent was obtained from all participants.

Study Parameters

Chromogenic LAL Assay of Serum Endotoxin

Before endoscopy, 79 of the enrolled subjects were subjected to blood sampling from a peripheral vein for endotoxin measurement. Blood samples were collected into sterile, pyrogen-free vials, and then serum was separated and stored at -80 °C until processed. Endotoxin concentration was determined in serum samples by the quantitative chromogenic Limulus Amebocyte Lysate test (LAL, QCL-1000, Lonza, Walkersville, MD, USA) via the microplate method and expressed in EU/mL, according to the manufacturer's instructions. The pH of samples was tested from an aliquot and was found to be within the range 6.0–8.0. In order to determine whether a product's intrinsic color might be of concern for LAL assay performance, 50 μL of sample with the addition of 150 μL LAL reagent water and 100 μL appropriate stop reagent, without incubation, were measured at 405–410 nm. If the absorbance was significantly greater than the absorbance of LAL reagent water, then these samples were tested after 1/10 dilution with LAL reagent water. The dilution factor was used in the final calculations for determining the concentration of endotoxin. All samples were analyzed in duplicate, by one operator using standard equipment under sterile and fixed operating conditions using pyrogen-free consumables. The coefficient of variation between the duplicate was 5.8%. Fifty microliters of each sample was mixed with the LAL, added in microplate well, and incubated at 37 °C for 10 min. The LAL sample was mixed with a chromogen, incubated at 37 °C for an additional 6 min, and then the reaction was stopped by a stop reagent. The concentration of endotoxin for every sample was calculated from a standard curve, created in the same run, by the absorbance of the sample endotoxin solutions and was determined spectrophotometrically at 405 nm, in direct proportion to the amount of endotoxin present.

Histopathological Evaluation

Duodenal biopsies were fixed in 10% neutral buffered formalin, embedded in paraffin, sectioned at 4 μm, and stained with hematoxylin and eosin (Fig. 1b).

Histochemical Detection of Paneth Cells

For identification of Paneth cells, phloxine-tartrazine histochemical staining was used, at the standard protocol procedure. Sections were stained with phloxine-tartrazine (Lendrum's Phloxine-Tartrazine Kit, Clin-Tech Ltd, UK), according to the Lendrum reaction [26]. Briefly, paraffin sections were dewaxed in xylene, hydrated through graded alcohols to water, and the nuclei were stained blue with Mayer's hematoxylin solution for 10 min. Subsequently, tissue sections were stained in 0.5% phloxine solution for 20 min, and differentiated in saturated tartrazine for up to 20 min. In Lendrum's phloxine-tartrazine method, the Paneth cell granules appeared red, while collagen and the background tissue turned in pale yellow (Fig. 1b).

Counting of Paneth Cells

For cell counts, 6–25 crypts were evaluated. Observation of positive for phloxine-tartrazine crypt epithelial cells and cell counting were performed by conventional light microscopy at a constant magnification (400×) and expressed as the number of Paneth cells per crypt.

Human α-Defensins 5, 6

Immunohistochemistry was performed on 4-μm-thick formalin-fixed, paraffin-embedded (FFPE) tissue sections, mounted on adhesive glass slides. After deparaffinization and rehydration through xylene and graded ethanol to distilled water, heat-induced epitope retrieval was performed. FFPE tissue slides from biopsies were used for staining with the primary antibodies for HD5 (Anti-DEFA5, HPA015775, Sigma, St Louis, MO), HD6 (Anti-DEFA6, HPA019462, Sigma, St Louis, MO) at a dilution of 1:2500 and 1:3000, respectively. HD5 and HD6 proteins were visualized by a horseradish peroxidase-conjugated detection system, followed by incubation with 3′-diaminobenzidine tetrahydrochloride (Dako). Harris hematoxylin counterstaining was performed to visualize the cell nuclei (Fig. 1a).

For the immunohistochemical evaluation, the following algorithm was implemented: The total number of Paneth cells was counted on 6–25 crypts, depending on the sample size. The immunohistochemical intensity of
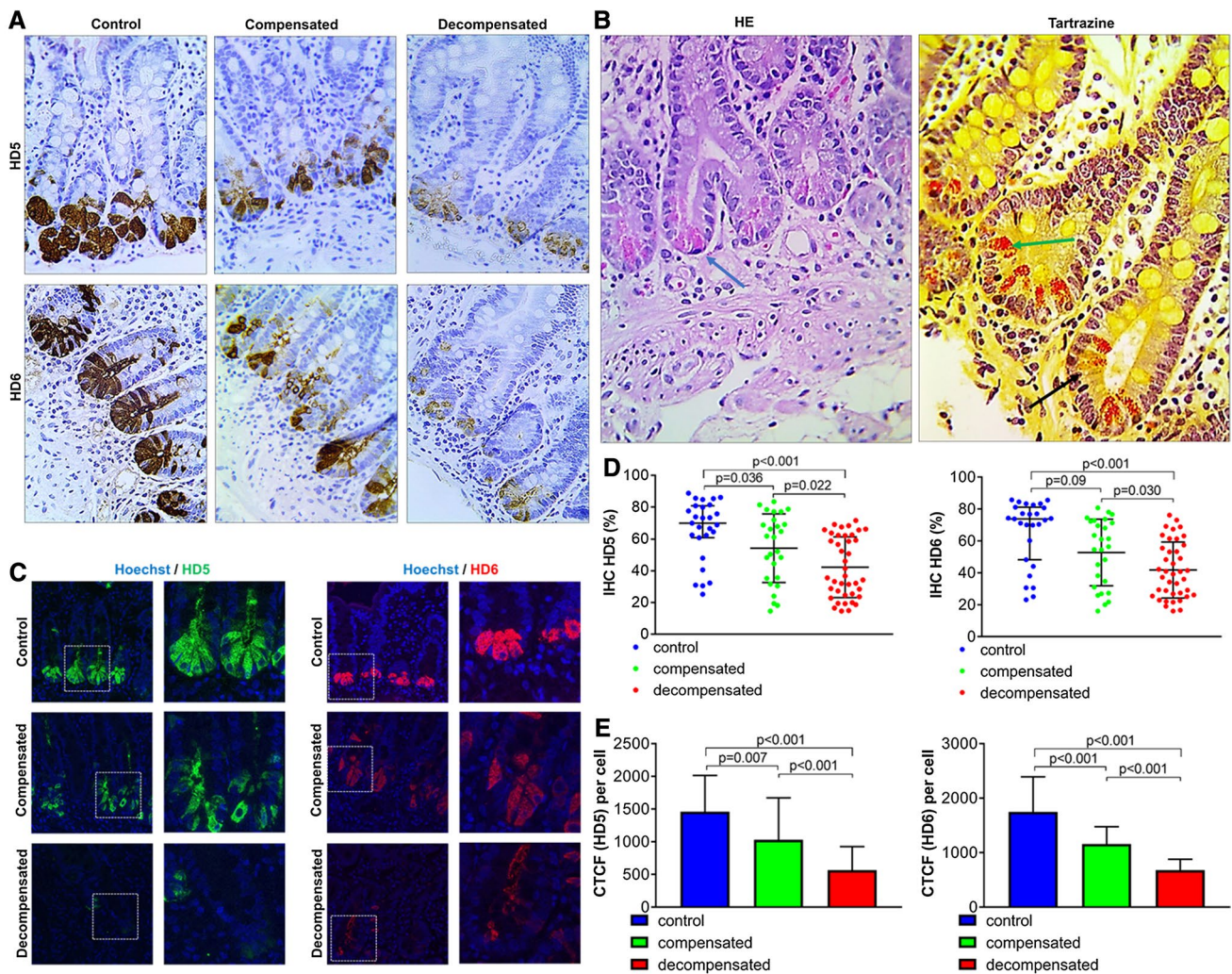
Fig. 1 Human a-defensins 5 (HD5) and 6 (HD6) immunohistochemical stain and immunofluorescence. Sections stained with anti-DEFA5 and anti-DEFA6 antibodies, from the small intestine of healthy subjects, showing strong immunoreactivity of Paneth cells, in contrast to the weak immunostaining of sections in cirrhotic patients (**a**). Paneth cells stained with hematoxylin–eosin and phloxine-tartrazine histochemical stain (**b**). Paneth cells, which have an empty appearance due to granule depletion (black arrow). Normal Paneth cell granules with plump eosinophilic granules (green arrow). Original magnification ×400 (IHC). Paneth cells with varying fluorescent intensities following immunofluorescence for HD5 or HD6 (**c**). Original magnification ×630 (IF). Dot—plot diagrams and bar charts (GraphPad Prism 7.04) representing α-defensin expression are shown and black lines respond to the median value and the interquartile range which contains the 50% of values (**d**, **e**). The p value in each diagram refers to the Mann–Whitney test analyzing data as continuous variables

α-defensins was scored for each cell as mild immunoreactivity (weak immunostain scattered within the Paneth cell cytoplasm) and strong (intense immunostain uniformly distributed within the entire Paneth cell cytoplasm). For each case, the expression of α-defensins was calculated by dividing the number of strong immunoreactive Paneth cells with the total Paneth cells number. The extent of immunoreactivity was scored on a three-point scale from 1 up to 3. A proportion of strong immunoreactive Paneth cells of 0–30% was considered as +1 (severely depleted), 30–60% as +2 (mildly depleted), and ≥ 60% + 3 (normal).

Immunofluorescence

Immunofluorescence for α-defensins 5, 6 was performed on paraffin-embedded sections (4 μm thick) from duodenal tissue. After deparaffinization and rehydration through xylene and graded ethanol to distilled water, tissue sections were fixed with ice-cold methanol for 10 min (− 20 °C). Slides were stained using the rabbit primary antibodies for HD5 (Anti-DEFA5, rabbit polyclonal, IgG isotype, HPA015775, Sigma, St. Louis, MO) and HD6 (Anti-DEFA6, rabbit polyclonal, IgG isotype, HPA019462, Sigma, St. Louis, MO) of

1:2000 dilution in blocking buffer for 1 h at room temperature. Subsequently, sections were incubated with the appropriate secondary fluorescent antibodies against α-defensins 5, 6 (goat anti-rabbit IgG (H + L) cross-adsorbed secondary antibody, Alexa Fluor 568, Invitrogen®, Camarillo, CA, USA, and goat anti-rabbit IgG (H + L) secondary antibody, Alexa Fluor 488, Invitrogen®, Camarillo, CA, USA), diluted 1:1000 in blocking buffer for 1 h at room temperature. The slides were mounted using Mowiol 4-88 (Calbiochem) medium with bisbenzimide H 33258 solution (Hoechst 33258, 1:1500, Sigma), a water-soluble adenine–thymine selective DNA fluorescent stain. An isotype control was used to ensure antibody specificity in each staining. Tissue sections were evaluated with a confocal Leica SP5 microscope, using 63× lens and digital images were processed and quantified with Fiji software (Fig. 1c). Immunofluorescence was performed in six cases from each group.

For determining the level of fluorescence, the Paneth cells, which represent the area of interest (ROI), were selected using the image J systems' selection tools and added to the ROI Manager. The predefined variables were set for area, integrated density, and mean gray value. The Multi-Measure/Multi-Plot tool was used to derive a stack of values for the selected cells. This step was repeated for the region next to Paneth cells that has no fluorescence (background). The corrected total cell fluorescence (CTCF) per Paneth cell was calculated using the following formula CTCF = integrated density − (area of selected cell x mean fluorescence of background readings).

Intraepithelial CD3+ T-lymphocytes

The number of IELs located within the epithelium, above the basal lamina, and between epithelial cells was determined. Stains for CD3 (anti-CD3: rabbit polyclonal Ab, Dako) were performed on 4-μm-thick FFPE tissue sections, using standard techniques. Five well-oriented villi were randomly selected per case, to evaluate the CD3+ cell infiltration. In each villus, the number of CD3+ IELs was counted firstly in the villus tip (defined as the top 20 enterocytes in the apical portion of the villus), named T, and secondly in the lateral segment of the villus (defined as the lateral 40 enterocytes on each side of the villus, totaling 80 enterocytes per villus), named S. In addition, for each villus, the number of CD3+ T cells was recorded over the total of 100 enterocytes, named V. Thus, the total number of CD3+ IELs in T, S, and V locations of the five analyzed villi resulted by adding the respective numbers counted on each villus and was expressed over 100 T enterocytes, 400 S enterocytes and 500 V enterocytes. In order to evaluate ratios, the V IELs/500 V enterocytes were converted to V IELs/100 V enterocytes. For statistical analysis, the total absolute number of IELs/100 T enterocytes and the absolute number of IELs/100 V enterocytes

were analyzed. In addition, the T IEL/V IEL ratio was calculated, exploring any specific distribution pattern along the villus axis (Fig. 2a).

CD20+ B-lymphocytes

CD20 expression using FFPE tissue was assessed using routine methods of staining with the L26 antibody (monoclonal mouse anti-human CD20cy, Clone L26, Isotype: IgG2a, kappa, Dako). The slides were examined using an optical microscope (Amscope T720QB, Irvine, CA, USA) fitted with a video camera (Amscope MU1000, Irvine, CA, USA), and the images were analyzed using a digital image analysis software (ImageJ, version 1.48 Wayne Rasband, National Institutes of Health, Bethesda, MD, USA) by image thresholding, a method of picture segmentation that isolates objects by converting grayscale images into binary images. Histogram, a common thresholding algorithm, represents the distribution of pixel intensities in the image. A pixel with an intensity of 0 represents black color, a pixel with a value of 255 represents white, and everything in between is a shade of gray. In our study, we semiautomatically applied the "Default," a modified IsoData, thresholding method. After displaying the threshold values in red mode and by dragging the sliders, different regions within the grayscale were interactively selected, so that pixels in the image which fell in the selected range were highlighted in red (Fig. 2c–f).

Three images of each section were captured at standard frame setting (3584×2748 pixels, RGB, 24-bit depth, 38 MB), with a magnification of 10×. CD20+ B-lymphocytes scattered or aggregates were quantified by digital image analysis in an area of 3 mm^2 and were expressed as an area fraction after image thresholding. Area fraction represents the percentage of pixels in the image that have been highlighted in red, which means that only thresholded pixels are included in measurement calculations.

Morphometric Analysis

Five villi and crypts of Lieberkühn from duodenal biopsies were measured with an optical microscope (Amscope T720QB, Irvine, CA, USA) and a digital camera (Amscope MU1000, Irvine, CA, USA) using ToupView, a video-capturing software (Amscope, Irvine, CA, USA). The following variables were measured: villus height, crypt depth, and the villus height-to-crypt depth ratio. An average value was calculated for each parameter (Fig. 2b).

Statistical Analysis

Statistical analysis was performed using SPSS 24.0 for Windows software (SPSS Inc, Chicago, IL). Continuous data were expressed as mean ± standard deviation or median
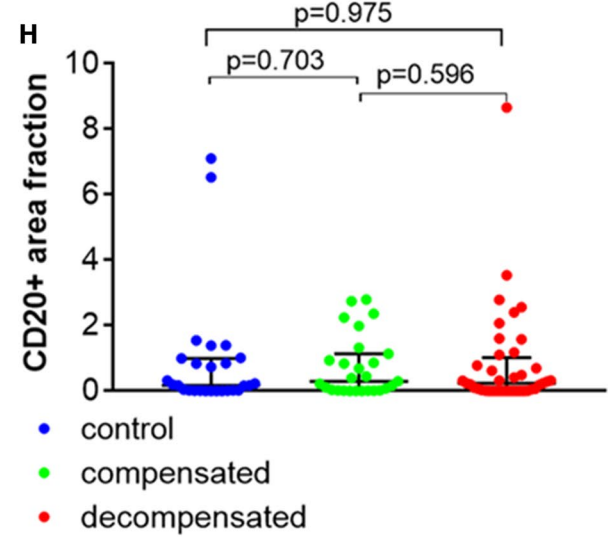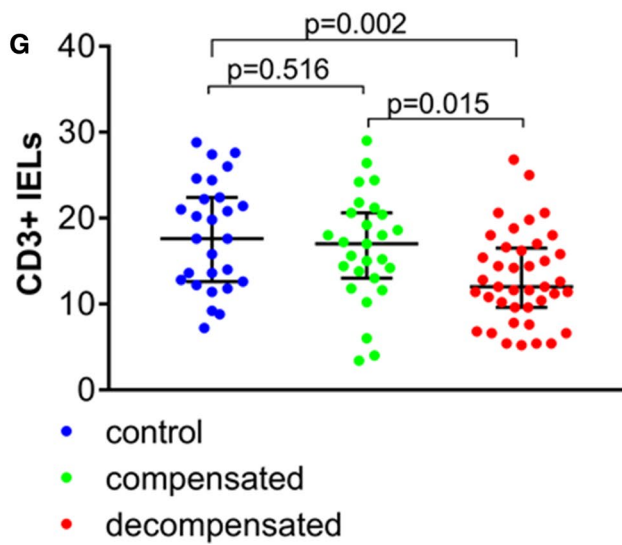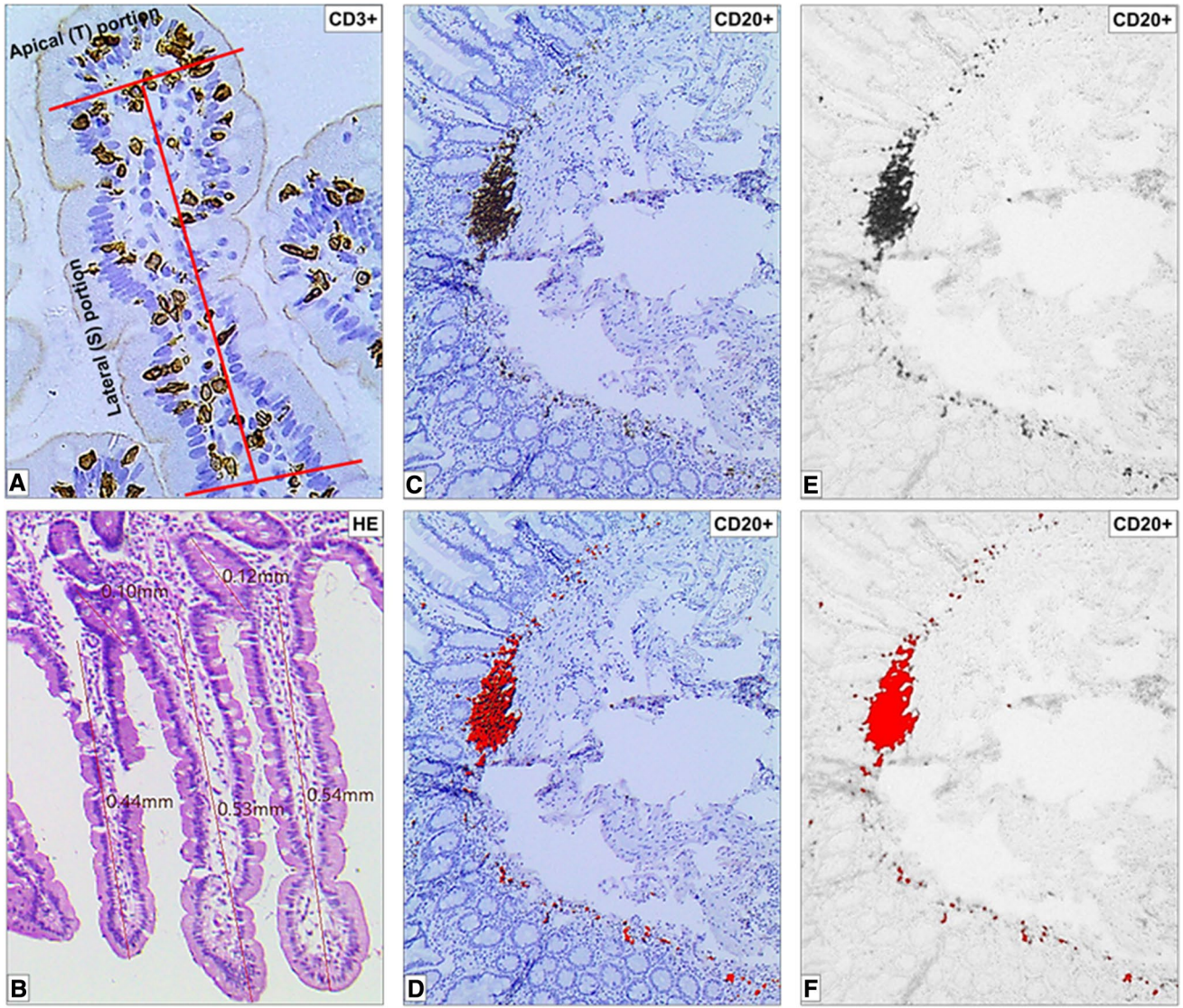
◀**Fig. 2** CD3+ intestinal IELs counted both in the lateral (S) and the apical villus portion (T). (**a**, original magnification ×400). Villi height and crypt depth measured by digital morphometric analysis (**b**, original magnification ×200). CD20+ B-lymphocytes infiltrate within the lamina propria (**c**, original magnification ×100), and CD20+ B-lymphocytes area fraction after image segmentation (**d**–**f**, original magnification ×100). Dot—plot diagrams (GraphPad Prism 7.04) representing CD3+ intestinal IELs count (**g**) and CD20+ B-lymphocytes infiltrate within the lamina propria (**h**) are shown and black lines respond to the median value and the interquartile range which contains the 50% of values. The *p* value in each diagram refers to the Mann–Whitney test analyzing data as continuous variables

(interquartile range). Data were analyzed by nonparametric Mann–Whitney test and Kruskal–Wallis when comparisons of more than two groups were performed. Univariate and multivariate linear regression analyses were used to explore the effects of HD5 and HD6 expression as well as IELs count on serum endotoxin concentration. Correlation analysis was performed to evaluate the association between the endotoxin levels and the other measured variables by Spearman's test. Probability values (two sided) were considered to indicate statistical significance at $p < 0.05$.

Results

Serum Endotoxin

All subjects had detectable levels of endotoxin in their serum at baseline measurement with a median endotoxin concentration of 0.450 EU/mL (IQR 0.370–0.560 EU/mL). Serum endotoxin was higher in cirrhotic patients (0.475 EU/mL, IQR 0.430–0.598 EU/mL) as compared to healthy controls (0.330 EU/mL, IQR 0.290–0.385 EU/mL) ($p < 0.0001$) and that observation was more profound among decompensated (0.508 EU/mL, IQR 0.446–0.701 EU/mL) than healthy subjects ($p < 0.0001$). In addition, there was a significantly higher concentration of serum endotoxin in the group of decompensated versus compensated patients (0.410 EU/mL, IQR 0.366–0.499 EU/mL) ($p = 0.000189$).

Regarding the decompensated group of patients, the endotoxin levels are parallel to MELD-sodium score, using a MELD-sodium score equal to 20 as a cutoff. In intragroup analysis, the prevalence of endotoxemia was significantly higher among decompensated patients with MELD-sodium score ≥ 20 (0.595 EU/mL, IQR 0.506–0.844 EU/mL) when compared to the subgroup with MELD-sodium score < 20 (0.455 EU/mL, IQR 0.441–0.614 EU/mL) ($p = 0.005$).

Significant differences were found regarding the presence of clinically overt portal hypertension, as evidenced by the presence of esophageal varices ($p = 0.003$), their size (F1/F2/F3, $p = 0.036$), portal hypertensive gastropathy ($p = 0.001$), and platelet count (≥ 92,000 vs < 92,000, $p = 0.001$).

Endotoxin concentration was increased with higher ascites grade (G1/G2/G3, $p = 0.013$) (Table 2).

Paneth Cell Counts

Paneth cells showed consistent granule morphology, with each cell full of eosinophilic granules. Sections from the second portion of duodenum showed little variation in the number of Paneth cells per crypt among cirrhotic patients (3.3, IQR 2.7–3.9) and healthy controls (3.5, IQR 2.6–4.1) ($p = 0.643$). Paneth cell counts in the duodenal crypts were comparable in sections from normal and diseased small intestine, but reduced in sections among cirrhotic patients with a larger size of esophageal varices (F1/F2/F3, $p = 0.023$). However, this observation cannot be considered constant and reproducible since significant differences were not observed among the other parameters that are indicative of clinically overt portal hypertension, namely platelet count < 92,000 ($p = 0.947$), the presence of portal hypertensive gastropathy ($p = 0.106$) and gastric varices ($p = 0.193$). Furthermore, in the subanalysis of the decompensated group of patients, the Paneth cell counts were comparable between patients with a different MELD-sodium (≥ 20 vs < 20, $p = 0.689$) or Child–Pugh score (C vs B, $p = 0.473$).

Expression of Intestinal α-Defensins 5, 6

The Paneth cells from patients with liver cirrhosis appeared to be depleted of granules as compared to normal controls. Concerning the expression of HD5 and HD6 within the group of healthy population, 77.8 and 74.1%, respectively, exhibit normal expression of the peptides, while 22.2 and 25.9% show depleted expression either mild or severe. On the other hand, 37.3 and 32.8% of cirrhotic patients exhibit a normal type of HD5, HD6 intestinal expression, and the remaining 62.7 and 67.2%, respectively, represent decreased peptides expression (Table 3). This depletion was confirmed on immunohistochemistry using the anti-DEFA5 ($p = 0.000287$) and anti-DEFA6 antibodies ($p = 0.000314$), analyzing data in accordance with the described scoring method. The downregulation in HD5, HD6 expression was also apparent between the subgroups of compensated cirrhotic patients and healthy subjects ($p = 0.040$, $p = 0.043$, respectively), but was more profound comparing the decompensated group to healthy ($p = 0.000035$, $p = 0.000040$, respectively). We also noted a widespread downregulation of α-defensins 5 and 6 in the subgroup of decompensated patients as compared to compensated patients ($p = 0.025$, $p = 0.041$, respectively). An inverse correlation of intestinal HD5 and HD6 expression with endotoxemia was documented (r = − 0.790, $p < 0.0001$, r = − 0.777, $p < 0.0001$, respectively). Data were also confirmed by immunofluorescence analysis, as

Table 2 Serum endotoxin concentration among distinct subgroups of cirrhotic patients regarding to the clinical parameters representative of different disease stages and portal hypertension presence

	n	Mean ± SD	Median (IQR)	p
Patients status				
Healthy	19	0.344 ± 0.083	0.330 (0.290–0.385)	<.0001
Cirrhosis	60	0.533 ± 0.166	0.475 (0.430–0.598)	
Cirrhosis status				
Compensated	20	0.435 ± 0.086	0.410 (0.366–0.499)	.000189
Decompensated	40	0.583 ± 0.175	0.508 (0.446–0.701)	
MELD-Na				
< 20	24	0.527 ± 0.146	0.455 (0.441–0.614)	.005
≥ 20	16	0.666 ± 0.187	0.595 (0.506–0.844)	
CP score				
A	20	0.435 ± 0.086	0.410 (0.366–0.499)	.000028
B	21	0.513 ± 0.138	0.455 (0.438–0.558)	
C	19	0.660 ± 0.183	0.600 (0.505–0.825)	
Ascites grade				
G1	13	0.474 ± 0.059	0.450 (0.438–0.485)	.003
G2/G3	27	0.635 ± 0.189	0.590 (0.475–0.745)	
Ascites grade				
G1	13	0.474 ± 0.059	0.450 (0.438–0.485)	.013
G2	20	0.623 ± 0.188	0.580 (0.476–0.724)	
G3	7	0.669 ± 0.202	0.740 (0.445–0.850)	
PLTs				
≥ 92,000	39	0.473 ± 0.101	0.450 (0.420–0.505)	.001
< 92,000	21	0.645 ± 0.205	0.640 (0.488–0.785)	
EV				
Yes	48	0.560 ± 0.173	0.503 (0.445–0.640)	.003
No	12	0.425 ± 0.065	0.425 (0.390–0.454)	
EV size				
F1	16	0.494 ± 0.114	0.450 (0.414–0.561)	.036
F2	15	0.555 ± 0.195	0.500 (0.430–0.640)	
F3	17	0.627 ± 0.183	0.570 (0.478–0.785)	
EV size				
F1	16	0.494 ± 0.114	0.450 (0.414–0.561)	.053
F2/F3	32	0.593 ± 0.189	0.513 (0.451–0.728)	
PHG				
Yes	38	0.587 ± 0.183	0.533 (0.444–0.711)	.001
No	22	0.441 ± 0.068	0.445 (0.391–0.495)	
Gastric varices				
Yes	7	0.780 ± 0.192	0.825 (0.640–0.960)	.001
No	53	0.501 ± 0.134	0.455 (0.423–0.563)	

MELD Model for End-Stage Liver Disease, *CP score* Child–Pugh score, *PLTs* platelets, *EV* esophageal varices, *PHG* portal hypertensive gastropathy, *IQR* interquartile range, *SD* standard deviation

adjusted total cell fluorescence intensity of α-defensins 5, 6 in Paneth cells was found higher among healthy subjects when compared to cirrhotic patients ($p < 0.0001$).

Table 3 HD5, HD6 expression of Paneth cells within distinct groups of cirrhotic patients and healthy

	Control	Compensated	Decompensated
HD5			
Severely depleted granules	1	4	14
Mildly depleted granules	5	9	15
Normal	21	14	11
HD6			
Severely depleted granules	2	6	15
Mildly depleted granules	5	8	16
Normal	20	13	9

HD5 Human α-defensin 5, *HD6* Human α-defensin 6

Immunological Changes of Gut-Associated Lymphoid Tissue

We demonstrated that cellular immunity of intestinal mucosa was deficient regarding CD3+ IELs, while CD20+ B-lymphocytes population as expressed by area fraction index (0.24, IQR 0.01–1.10 vs 0.17, IQR 0.01–1, respectively) was unaltered between the cirrhotic patients and healthy individuals ($p = 0.019$, $p = 0.871$, respectively).

More specifically, IELs were found compromised in count only in the group of decompensated patients (12, IQR 9.6–16.5 per 100 enterocytes) compared to compensated (17, IQR 13–20.6 per 100 enterocytes) and healthy individuals (17.6, IQR 12.6–22.4 per 100 enterocytes) ($p = 0.015$, $p = 0.002$, respectively). There were no significant changes of IELs, between the compensated patients and healthy ($p = 0.516$). Regarding the IELs distribution pattern along the villus axis, the estimated top-to-villus ratio of IELs was comparable among both investigated subgroups of decompensated (0.931, IQR 0.723–1.199) and compensated (1.060, IQR 0.833–1.250) cirrhotic patients as compared to healthy (1.029, IQR 0.802–1.107) ($p = 0.623$, $p = 0.494$, respectively). Despite the lower IELs count in the advanced liver disease patients, in the multivariate linear regression model analysis, the effect of the specific changes of IELs on endotoxin concentration did not reach statistical significance ($p = 0.097$, Table 4).

Morphometric Parameters

The median villus length was measured 0.56 mm (IQR 0.47–0.63 mm) among healthy, 0.51 mm (IQR 0.46–0.61 mm) for compensated patients, and 0.48 mm (IQR 0.39–0.59 mm) in decompensated patients' groups. The villus height was significantly shorter in the decompensated disease group as compared to the normal group ($p = 0.027$), while this observation was not reproduced when comparing

Table 4 Predictive models of endotoxin serum levels related to HD5, HD6 expression and CD3+ IELs count

	Univariate linear regression		Multivariate linear regression	
	β (95% CI)	p	β (95% CI)	p
HD5/endotoxin	−0.804 (−0.07, −0.05)	<.0001	−0.445 (−0.006, −0.001)	.010
HD6/endotoxin	−0.786 (−0.07, −0.05)	<.0001	−0.348 (−0.005, −0.000166)	.038
IELs/endotoxin	−0.365 (−0.015, −0.004)	.001	−0.119 (−0.007, 0.001)	.097

Univariate and multivariate linear regression analyses were used to explore the effects of HD5 and HD6 expression as well as IELs count on serum endotoxin concentration

HD5 human α-defensin 5, *HD6* human α-defensin 6, *IELs* intraepithelial lymphocytes, *CI* confidence interval

to the compensated patients ($p = 0.109$). Crypts length and the ratio of villus height to crypt depth were not affected enough to reach at statistical significance level among all the groups ($p = 0.307$, $p = 0.610$, respectively).

Discussion

The alimentary tract hosts a dynamic ecosystem of microorganisms and sets a unique cross talk between local immune system, immune effector cells, intestinal epithelium, and inhabiting microbes, forming a physical barrier against luminal invaders and toxins. The migration of microorganisms or their pathogen-associated molecular patterns (PAMPs), such as lipopolysaccharide, from the intestinal lumen to the mesenteric lymph nodes (MLNs), systemic circulation, and other normally sterile extra-intestinal tissues, is termed bacterial translocation. A series of experimental studies have shown that passage of bacteria and their byproducts across the intestinal barrier is a commonplace in liver cirrhosis [27]. Nevertheless, the precise underlying cellular and molecular pathways implicated in the phenomenon of microbial translocation in liver cirrhosis have not been resolved yet [28].

The functional role of the Paneth cell, firstly described by Joseph Paneth in Vienna in 1888, has remained an enigma for more than 100 years. Recent data from Teltschik et al. strongly implicate the Paneth cell as a key effector in the host immune response to enteric bio-pathogens in experimental models of animals with cirrhosis, as have shown significantly compromised Paneth cell antimicrobial host defense, although findings from another study did not assert a significant alteration at specific tissue level [29, 30].

The present study demonstrates reduced HD5 and HD6 expression by Paneth cells in patients with liver cirrhosis. This observation is more profound in advanced liver disease stages and is linked to disturbed mucosal intestinal barrier function and higher levels of serum endotoxin. Endotoxemia as a marker of increased intestinal permeability was found to be related to the presence of portal hypertension, assessed by the presence and size of esophageal varices, ascites, and platelet counts. Our findings concerning the deterioration

of intestinal barrier and increased bacterial translocation in view of the decompensation and progression to advanced stages of liver disease were in concordance with the results found in previous studies [31–33].

Moreover, we found that among patients with decompensated liver disease, endotoxin concentration was more increased in those patients with higher MELD-sodium score. Our findings corroborate the view of intestinal barrier dysfunction in cirrhotic patients and support the concept that the bacterial translocation parallels with the disease progression to more advanced stages.

Malnutrition in chronic liver disease may contribute to the compromised intestinal barrier function and can increase the incidence of spontaneous bacterial peritonitis [34, 35]. Experimental data from previous studies have recorded that immune-enhancing feeding favors the expression of mouse intestinal defensins [36].

Malnutrition, the subsequent zinc depletion, and alterations in bile secretion and the enterohepatic circle of bile acids, which occur in advanced cirrhosis according to data from previous studies, may account for the observed changes in α-defensin expression, given that zinc constitutes a vital element for Paneth cells [37–40].

Considering that the lymphoid tissues associated with the intestine are continuously exposed to antigens of the alimentary lumen [25], we hypothesized that among the possible mechanisms for deteriorated mucosal barrier and the subsequent increased intestinal permeability might be the impairment of GALT. To the best of our knowledge, this investigation constitutes the first assessment of the comprehensive role of the GALT, especially attending to IELs and lamina propria B-lymphocytes at duodenal specific tissue level among patients with liver cirrhosis.

As a potent cause of the fragility of the mucosal barrier, intestinal γδ T cell deficiency has been proposed in animal models [41]. In our study, depleted IELs in advanced liver cirrhosis represent a defective ability of T-lymphocytes to migrate at the frontiers of the intestinal mucosal barrier and combat the noxious invaders. However, in the multivariate linear regression analysis, the effect of IELs changes did not reach statistical significance, suggesting that further

investigation in this field is required. Nonetheless, this finding is in accordance with the suppression of lymphocytes chemotaxis and responsiveness to lipopolysaccharide (LPS) that has been recorded after exposure to ethanol [42]. In parallel with the findings of Kawakami et al., Choudhry et al. revealed that CD3+ T cell depletion in animals furthered the spread and accumulation of bacteria to MLNs, spleen, and blood circulation [43]. Regarding the B-lymphocyte population, our data do not confirm any changes between cirrhotic patients and healthy subjects.

Morphometric analysis revealed that villus and crypt architecture were preserved among the compensated patients, while in decompensated disease status, a relative shortening of villi was observed. The reduction in the height of villi among patients in decompensated disease status is consistent with the morphological changes discovered in other studies in cirrhotic mice, which have shown atrophic and shorter villi [44].

The consequences of intestinal immune dysfunction and the loss of local immunologic surveillance reflect systematically. The lack of homeostatic immunological mechanisms may decrease the intestinal barrier function, favoring the invasion of biomolecules derived from the cell wall of Gram-negative bacteria into the bloodstream, a condition named endotoxemia, which is the cornerstone of serious clinical aspects on the natural course of liver cirrhosis [45, 46].

However, we should comment that despite the significant research interest in the technical aspects of endotoxin measurement, there is no robust gold standard assay to directly test for endotoxemia. Furthermore, cirrhotic patients constitute a specific population with suppressed functional and synthetic liver capacity. C-reactive protein (CRP), lipopolysaccharide-binding protein (LBP), procalcitonin as indirect bacterial translocation (BT) markers are not ideal, as they are all downregulated in liver disease mitigating their clinical relevance to the BT, and the accuracy of these assays is dependent on hepatic function. Moreover, CRP, LBP, and procalcitonin are acute phase proteins that are mainly used to differentiate infection from non-infection—in this study current infection has been considered as an exclusion criterium. Additionally, at current, the other existing methods provide an indirect or semiquantitative evaluation of endotoxemia. For that reason, despite the possible limitations concerning the use of LAL assay in biological samples, in this study, we used this method that provides a direct quantification of endotoxin levels and has been widely validated in research studies [47–49].

In view of the results reported here, we demonstrate that the derangement of host-bacteria homeostasis in liver cirrhosis could be mediated by the relative deficiency of Paneth cell defensins. This deficit possibly affects the antibacterial host defense capacity and predisposes to a breakdown of the gut immune barrier. This study supports the hypothesis that intestinal AMPs expression is affected in cirrhotic patients, leading to defective intestinal integrity and enhanced bacterial translocation.

Compliance with ethical standards

Conflict of interest The authors declare that they have no conflicts of interest.

References

1. Turner JR. Intestinal mucosal barrier function in health and disease. *Nat Rev Immunol*. 2009;9:799–809.
2. Assimakopoulos SF, Tsamandas AC, Tsiaoussis GI, et al. Altered intestinal tight junctions' expression in patients with liver cirrhosis: a pathogenetic mechanism of intestinal hyperpermeability. *Eur J Clin Invest*. 2012;42:439–446.
3. Johansson ME, Ambort D, Pelaseyed T, et al. Composition and functional role of the mucus layers in the intestine. *Cell Mol Life Sci*. 2011;68:3635–3641.
4. Ouellette AJ, Selsted ME. Paneth cell defensins: endogenous peptide components of intestinal host defense. *FASEB J*. 1996;10:1280–1289.
5. Dinsdale D. Ultrastructural localization of zinc and calcium within the granules of rat Paneth cells. *J Histochem Cytochem*. 1984;32:139–145.
6. Podany AB, Wright J, Lamendella R, Soybel DI, Kelleher SL. WriZnT2-mediated zinc import into Paneth cell granules is necessary for coordinated secretion and Paneth cell function in mice. *Cell Mol Gastroenterol Hepatol.*. 2016;2:369–383.
7. Porter EM, Liu L, Oren A, Anton PA, Ganz T. Localization of human intestinal defensin 5 in Paneth cell granules. *Infect Immun*. 1997;65:2389–2395.
8. Bevins CL. The Paneth cell and the innate immune response. *Curr Opin Gastroenterol.*. 2004;20:572–580.
9. Wehkamp J, Chu H, Shen B, et al. Paneth cell antimicrobial peptides: topographical distribution and quantification in human gastrointestinal tissues. *FEBS Lett*. 2006;580:5344–5350.
10. Cash HL, Whitham CV, Behrendt CL, Hooper LV. Symbiotic bacteria direct expression of an intestinal bactericidal lectin. *Science*. 2006;313:1126–1130.
11. Peeters T, Vantrappen G. The Paneth cell: a source of intestinal lysozyme. *Gut*. 1975;16:553–558.
12. Nguyen LT, Haney EF, Vogel HJ. The expanding scope of antimicrobial peptide structures and their modes of action. *Trends Biotechnol*. 2011;29:464–472.
13. Bevins CL, Martin-Porter E, Ganz T. Defensins and innate host defence of the gastrointestinal tract. *Gut*. 1999;45:911–915.
14. Leitch GJ, Ceballos C. A role for antimicrobial peptides in intestinal microsporidiosis. *Parasitology*. 2009;136:175–181.
15. Gounder AP, Wiens ME, Wilson SS, Lu W, Smith JG. Critical determinants of human alpha-defensin 5 activity against non-enveloped viruses. *J Biol Chem*. 2012;287:24554–24562.
16. Johnson CA, Rachakonda G, Kleshchenko YY, et al. Cellular response to *Trypanosoma cruzi* infection induces secretion of defensin alpha-1, which damages the flagellum, neutralizes

trypanosome motility, and inhibits infection. *Infect Immun*. 2013;81:4139–4148.

17. Preet S, Bharati S, Shukla G, Koul A, Rishi P. Evaluation of amoebicidal potential of Paneth cell cryptdin-2 against *Entamoeba histolytica*. *PLoS Negl Trop Dis*. 2011;5:e1386.

18. Mathew B, Nagaraj R. Variations in the interaction of human defensins with *Escherichia coli*: possible implications in bacterial killing. *PLoS ONE*. 2017;12:e0175858.

19. Chu H, Pazgier M, Jung G, et al. Human α-defensin 6 promotes mucosal innate immunity through self-assembled peptide nanonets. *Science*. 2012;337:477–481.

20. de Leeuw E, Burks SR, Li X, Kao JP, Lu W. Structure-dependent functional properties of human defensin 5. *FEBS Lett*. 2007;581:515–520.

21. Albillos A, Lario M, Álvarez-Mon M. Cirrhosis-associated immune dysfunction: distinctive features and clinical relevance. *J Hepatol*. 2014;61:1385–1396.

22. Guy-Grand D, Malassis-Seris M, Briottet C, Vassalli P. Cytotoxic differentiation of mouse gut thymodependent and independent intraepithelial T lymphocytes is induced locally. Correlation between functional assays, presence of perforin and granzyme transcripts, and cytoplasmic granules. *J Exp Med*. 1991;173:1549–1552.

23. Taguchi T, Aicher WK, Fujihashi K, et al. Novel function for intestinal intraepithelial lymphocytes. Murine CD3+, gamma/delta TCR+ T cells produce IFN-gamma and IL-5. *J Immunol.*. 1991;147:3736–3744.

24. Yamamoto M, Fujihashi K, Amano M, McGhee JR, Beagley KW, Kiyono H. Cytokine synthesis and apoptosis by intestinal intraepithelial lymphocytes: signaling of high density alpha beta T cell receptor+ and gamma delta T cell receptor+ T cells via T cell receptor-CD3 complex results in interferon-gamma and interleukin-5 production, while low density T cells undergo DNA fragmentation. *Eur J Immunol*. 1994;24:1301–1306.

25. Inagaki-Ohara K, Dewi FN, Hisaeda H, et al. Intestinal intraepithelial lymphocytes sustain the epithelial barrier function against Eimeria vermiformis infection. *Infect Immun*. 2006;74:5292–5301.

26. Lendrum AC. The phloxine-tartrazine method as general histological stain and for the demonstration of inclusion bodies. *J Pathol Bacteriol.*. 1947;1947:399–404.

27. Thalheimer U, De Iorio F, Capra F, et al. Altered intestinal function precedes the appearance of bacterial DNA in serum and ascites in patients with cirrhosis: a pilot study. *Eur J Gastroenterol Hepatol.*. 2010;22:1228–1234.

28. Tsiaoussis GI, Assimakopoulos SF, Tsamandas AC, Triantos CK, Thomopoulos KC. Intestinal barrier dysfunction in cirrhosis: current concepts in pathophysiology and clinical implications. *World J Hepatol.*. 2015;7:2058–2068.

29. Teltschik Z, Wiest R, Beisner J, et al. Intestinal bacterial translocation in rats with cirrhosis is related to compromised Paneth cell antimicrobial host defense. *Hepatology*. 2012;55:1154–1163.

30. Kaltsa G, Bamias G, Siakavellas SI, et al. Systemic levels of human β-defensin 1 are elevated in patients with cirrhosis. *Ann Gastroenterol.*. 2016;29:63–70.

31. Merli M, Lucidi C, Pentassuglio I, et al. Increased risk of cognitive impairment in cirrhotic patients with bacterial infections. *J Hepatol*. 2013;59:243–250.

32. Goulis J, Patch D, Burroughs AK. Bacterial infection in the pathogenesis of variceal bleeding. *Lancet*. 1999;353:139–142.

33. El-Naggar MM, Khalil ELSA, El-Daker MA, Salama MF. Bacterial DNA and its consequences in patients with cirrhosis and culture-negative, non-neutrocytic ascites. *J Med Microbiol.*. 2008;57:1533–1538.

34. Zhou QQ, Yang DZ, Luo YJ, Li SZ, Liu FY, Wang GS. Overstarvation aggravates intestinal injury and promotes bacterial and endotoxin translocation under high-altitude hypoxic environment. *World J Gastroenterol*. 2011;17:1584–1593.

35. Casafont F, Sánchez E, Martín L, Agüero J, Romero FP. Influence of malnutrition on the prevalence of bacterial translocation and spontaneous bacterial peritonitis in experimental cirrhosis in rats. *Hepatology*. 1997;25:1334–1337.

36. Froy O, Levkovich G, Chapnik N. Immunonutrition enhances the expression and secretion of mouse intestinal defensins. *Gut*. 2006;55:900–901.

37. Hodin CM, Lenaerts K, Grootjans J, et al. Starvation compromises Paneth cells. *Am J Pathol*. 2011;179:2885–2893.

38. Kelly P, Feakins R, Domizio P, et al. Paneth cell granule depletion in the human small intestine under infective and nutritional stress. *Clin Exp Immunol*. 2004;135:303–309.

39. Mangray S, Zweit J, Puri P. Zinc deficiency in cirrhosis: micronutrient for thought? *Dig Dis Sci*. 2015;60:2868–2870.

40. Tremblay S, Romain G, Roux M, et al. Bile acid administration elicits an intestinal antimicrobial program and reduces the bacterial burden in two mouse models of enteric infection. *Infect Immun.*. 2017;85:e00942-16.

41. Inagaki-Ohara K, Chinen T, Matsuzaki G, et al. Mucosal T cells bearing TCR gamma delta play a protective role in intestinal inflammation. *J Immunol.*. 2004;173:1390–1398.

42. Kawakami M, Switzer BR, Herzog SR, Meyer AA. Immune suppression after acute ethanol ingestion and thermal injury. *J Surg Res*. 1991;51:210–215.

43. Choudhry MA, Fazal N, Goto M, Gamelli RL, Sayeed MM. Gut-associated lymphoid T cell suppression enhances bacterial translocation in alcohol and burn injury. *Am J Physiol Gastrointest Liver Physiol*. 2002;282:G937–G947.

44. Wen JB, Zhu FQ, Chen WG, et al. Oxymatrine improves intestinal epithelial barrier function involving NF-κB-mediated signaling pathway in CCl4-induced cirrhotic rats. *PLoS ONE*. 2014;9:e106082.

45. Maranduba CM, De Castro SB, de Souza GT, et al. Intestinal microbiota as modulators of the immune system and neuroimmune system: impact on the host health and homeostasis. *J Immunol Res.*. 2015;2015:931574.

46. Hooper LV, Littman DR, Macpherson AJ. Interactions between the microbiota and the immune system. *Science*. 2012;336:1268–1273.

47. Alexopoulou A, Agiasotelli D, Vasilieva LE, Dourakis SP. Bacterial translocation markers in liver cirrhosis. *Ann Gastroenterol.*. 2017;30:486–497.

48. Koutsounas I, Kaltsa G, Siakavellas SI, Bamias G. Markers of bacterial translocation in end-stage liver disease. *World J Hepatol.*. 2015;7:2264–2273.

49. Grube BJ, Cochane CG, Ye RD, et al. Lipopolysaccharide binding protein expression in primary human hepatocytes and HepG2 hepatoma cells. *J Biol Chem*. 1994;269:8477–8482.